Chemically modified guar gum and ethyl acrylate composite as a new corrosion inhibitor for reduction in hydrogen evolution and tubular steel corrosion protection in acidic environment

Ambrish Singh [a], K.R. Ansari [b,*], M.A. Quraishi [b], Savaş Kaya [c], Sultan Erkan [d]

[a] School of New Energy and Materials, Southwest Petroleum University, Chengdu, Sichuan, 610500, PR China
[b] Center of Research Excellence in Corrosion, Research Institute, King Fahd University of Petroleum and Minerals, Dhahran, 31261, Saudi Arabia
[c] Sivas Cumhuriyet University, Health Services Vocational School, Department of Pharmacy, Sivas, 58140, Turkey
[d] Yıldızeli Vocational School, Chemical and Chemical Company Technology, Cumhuriyet University, Sivas, Turkey

HIGHLIGHTS

- The inhibition efficiency of GG and GG-EEA is 92.3% and 77.5%.
- EIS suggests kinetically controlled corrosion process.
- The results of PDP proposed that GG-EEA is the mixed type of inhibitor.
- SEM, EDX, AFM and XPS studies confirmed GG-MMA adsorption.
- DFT and MC supports the experimental results.

ARTICLE INFO

ABSTRACT

The paper deals with the synthesis of Guar gum and ethyl acrylate (GG-EEA) composite. The synthesized natural polysaccharide composite was used as a corrosion inhibitor to reduce hydrogen evolution and P110 steel corrosion protection in 15% HCl (Hydrochloric acid). The primary corrosion techniques like weight loss, electrochemical impedance spectroscopy (EIS), and potentiodynamic polarization (PDP) was used to analyze the corrosion inhibition process. The PDP proposed that GG-EEA composite is a mixed-type corrosion inhibitor and inhibits corrosion by blocking the active sites presenting over the metal surface. The corrosion inhibition performance of GG alone is 77.5%, and that of GG-EEA is 92.3% at 500 mg/L. The adsorption of GG-EEA onto P110 steel is spontaneous and mixed type, i.e., both physical and chemical. The conformation of GG-EEA molecule adsorption was done using a scanning electron microscope (SEM), Energy dispersive x-ray spectroscopy (EDX), Atomic force microscopy (AFM), and X-ray photoelectron spectroscopy studies. Density functional theory (DFT) analysis was done to explore the active sites over the inhibitor in metal-inhibitor interaction. Molecular dynamic simulation (MD) simulations study reveals that GG-EEA has more adsorption capacity than GG alone.

Introduction

In the oil and gas industry, the selection of construction materials for pipelines casing and tubing is essential, and it depends on corrosion resistance, cost, and metallurgical properties. The strong mechanical strength of steel makes it the most suitable contraction material. The process of rejuvenating the old oil well is done by injecting the acid solution into the well, which causes the opening of the blocked pores and creates new pores. Among various acids, hydrochloric acid (15%) is preferably used for acidization because it readily dissolves rocks. However, in an aggressive environment (15% HCl), steel is prone to undergo corrosion. In the oil and gas industry, P110 steel is commonly used to construct tubing and casing pipes [1].

It is well known that the most effective way to control corrosion in acidic solution is the use of corrosion inhibitors. The survey of the literature reveals that the most effective corrosion inhibitors include organic compounds that include imidazole, thiazole, triazines, triazole, pyrazole, pyrimidines, hydrazine, Schiff bases, amino acids derivatives [2–9].

Nevertheless, toxicity and environmental risk is the prime drawback of many corrosion inhibitors. In the present time, the search for environmentally-friendly corrosion inhibitors is in demand. That is why corrosion scientists focus on developing very efficient, eco-friendly, and cost-effective corrosion inhibitors. Natural polymers and their derivatives, biopolymers, plant extracts, amino acids, etc., have been tested as eco-friendly corrosion inhibitors [10–22]. In 2008, Umoren studied the corrosion inhibition effect of Gum Arabic in 0.1 M H_2SO_4 solutions and obtained the inhibition efficiency (IE) of 21.84% and 79.69% for mild steel and aluminum, respectively at 0.5 g/L of inhibitor concentration [10]. Abdallah inhibition effect of studied Guar gum over carbon steel in 1 M H_2SO_4 solution and observed IE of 93.88% at 1500 mg/L [11]. Rajeswari et al. studied the inhibiting effects of glucose, gellan gum, and hydroxypropyl cellulose in 1 M HCl with the IE of 69.5%, 80.9%, 89.6% at 500 mg/L [12]. Li and Deng investigated Cassava starch graft copolymer's inhibition effect in H_2SO_4 and obtained IE of 95.7% at 100 mg/L [13]. Fiori-Bimbi group reported pectin's performance in 0.5 M HCl and obtained IE of 90.3% at 2 g/L [14]. Fares et al. studied Carrageenan's effect in 2 M HCl and obtained IE is 63.3% at 1600 mg/L [15]. In 2013, Bobina et al. showed L-histidine, an inhibitor for carbon steel corrosion in 0.5 M CH_3COOH/0.25 M CH_3COONa with IE of 81.6% 1550 mg/L [16]. Abiola and James analyzed Aloe vera leaves' extract in 2 M HCl with an IE of 67.1% at 10 %v/v [17]. Emranuzzaman et al. studied alcoholic extract of plant leaves and formaldehyde corrosion inhibitor for N80 steel in 15% HCl and obtained IE of 76.3% at 0.8% [18]. Matad group checked the corrosion inhibitive performance of Ketosulfone Drug as green inhibitor for mild steel in 1 M HCl and obtained IE of 96.6% at 200 mg/L [19]. In 2012 Eddy et al. used gum extracted from Daniella olliverri as corrosion inhibitor for mild steel in 0.1 M HCl, and IE obtained is 79.4% at 0.5 g/L [20]. Jyothi and Ravichandran studied the corrosive effect of Luffa aegyptiaca leaves extracted in 1 M HCl and obtained IE of 97.2% at 0.24 g/L [21]. Krishnaveni and Ravichandran [22] analyzed Morinda tinctoria leaf extract's performance as a corrosion inhibitor for

aluminum in 0.25 M H_2SO_4 and got the IE value of 71.5% at 19% v/v. A literature survey suggests that chemical modification of natural polysaccharides are better corrosion inhibitors that un-modified natural polysaccharides [23–26]. Banerjee et al. obtained the IE values of 58.1% and 91.8% for Polyacrylamide and polyacrylamide grafted with Okra mucilage, respectively, for the corrosion protection mild steel in H_2SO_4 solution [23]. Roy group has analyzed the corrosion inhibitive performance of Guar Gum (GG), and Polyacrylamide grafted guar gum (GG-g-PAM) over mild steel in 1 M HCl and obtained IE values of 71.4% (GG) and 90.7% (GG-g-PAM) at 500 g/L [24]. Biswas and groups tested Xanthan gum (XG) and xanthan gum-graft-poly (acrylamide) (XG-g-PAM) as mild steel corrosion inhibitor in 15% HCl. They gets the performance 90.8% (XG) and 93.1% (XG-g-PAM) at 0.5 g/L [25]. Similarly, Biswas et al. further compared the corrosion inhibitive performance of guar gum (GG) and chemically modified guar gum (CGG) for mild steel in 15% HCl and obtained the IE values of 86.5% (GG) and 95.3% (CGG) at 0.5 g/L [26].

In the present paper, the anticorrosive property of composite made by the guar gum's functionalization with ethyl acetoacetate (GG-EAA) was studied. The guar gum is a natural polysaccharide extracted from the seed of a leguminous family tree, i.e., Cyamopsis tetragonolobus. This tree is the native of India, Pakistan, and the North and South parts of America. Guar gum's unique property as a corrosion inhibitor is due to the water solubility, biodegradability, biocompatibility, and presence of heteroatoms. Guar gum is a galactomannan polysaccharide that consists of a straight chain of D-mannopyranosyl with (β(1 → 4) glycosidic linkage backbone and a side-chain of D-glucopyranosyl with (α(1 → 4) glycosidic linkage [27].

The present paper reveals the corrosion inhibition of chemically modified guar gum with ethyl acrylate (GG-EAA) for the corrosion inhibition of P110 steel in 15% HCl. The techniques used to investigate the corrosion protection ability of GG-EAA consist of weight loss, electrochemical impedance spectroscopy (EIS), and potentiodynamic polarization (PDP). The surface of P110 steel before and after the addition of GG-EAA was analyzed by scanning electron microscope (SEM), Energy Dispersive X Analysis (EDX), Atomic force microscopy (AFM). The experimental results were further strengthened by quantum chemical calculations (DFT) and molecular dynamic simulation (MD).

Experimental

Test sample and solution preparation

The composition of P110 steel consists of (wt.%): C = 0.26, Si = 0.19, Mn = 1.37, P = 0.004, S = 0.004, Cr = 0.148, Ni = 0.028, Cu = 0.019, Mo = 0.013, V = 0.006 and balanced Fe. The P110 steel dimension for the weight loss experiments is 2.5 cm × 2.0 cm × 0.2 cm, and for electrochemical experiments, the steel with rectangular shape was used with a 1 cm^2 exposed area. The SiC paper (grit size of 600–1200) was used to abrasion steel samples. The deionized water and ethanol were used for steel sample cleaning. Finally, the steel samples are

dried under warm air and kept in a desiccator. The corrosive medium, i.e., 15% HCl solution, was prepared from analytical grade HCl.

Inhibitor synthesis

First, 1 g of guar gum (GG) was slowly dissolved in 100 ml of distilled water. After that, 0.546 g of ascorbic acid and 4 g of ethyl acrylate (EEA) were respectively added to the guar gum solution, and after constant temperature reaction in a water bath at 35 °C for 30 min, 0.486 g of potassium persulfate (K$_2$S$_2$O$_8$) was added and continued at the same temperature for 1 h. After completing the reaction, an excess of acetone was added to the reaction product, and the resulting precipitate was separated by filtration and then dried under vacuum at 50 °C for 24 h. The desired product is a composite of gum with ethyl acrylate (GG-EAA). The composite of GG with EAA was confirmed using IR. The scheme of synthesis and molecular structure is represented in Fig. 1.

Weight loss measurements

The experiment of weight loss was done as per the ASTM standard [28]. The corrosion rate (C_R) was calculated by the following equation [29]:

$$C_R = \frac{8.76 \times 10^4 \times \Delta m}{s \times t \times \rho} \tag{1}$$

$$\eta\% = \frac{C_R - {}^{inh}C_R}{C_R} \times 100 \tag{2}$$

where C_R = corrosion rate (mm/y), s = P110 steel coupons area (cm^2), t = exposure duration (h), ρ = P110 steel density (gcm^{-3}) and Δm = change in weight loss (g). The C_R and ${}^{inh}C_R$ are the corrosion rates of P110 steel with and without inhibitor, respectively. All experiments were repeated three times to check the reproducibility of the results.
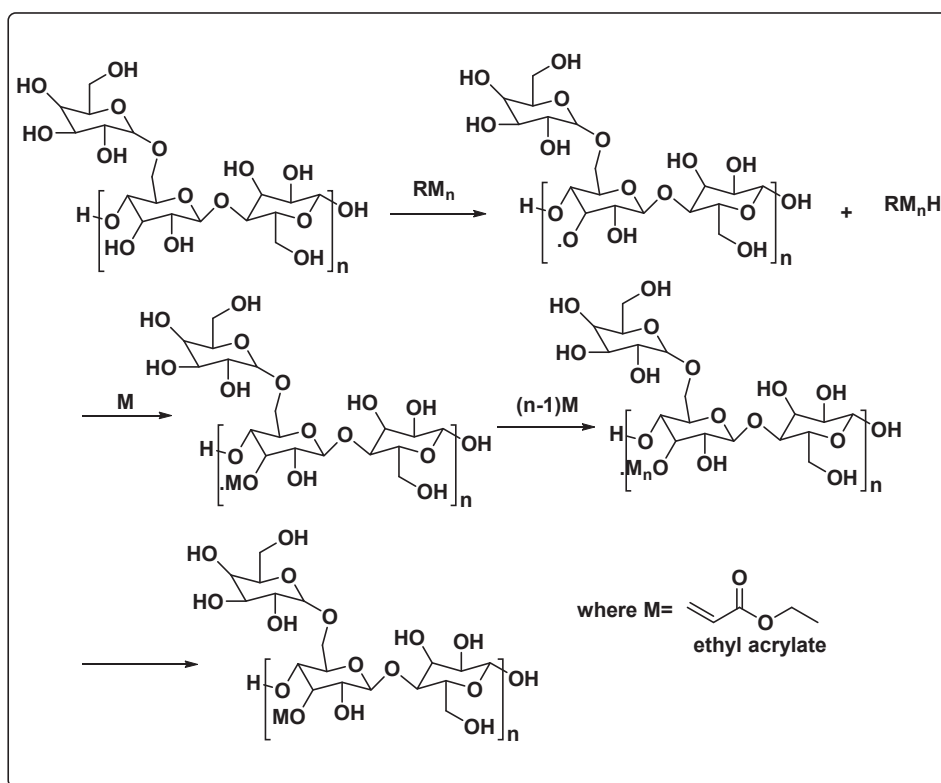

Fig. 1 – Synthesis scheme and molecular structure of (GG-EAA).

Electrochemical analysis

The measurements of electrochemical analysis were carried out using the Autolab Potentiostat device applying the three-electrode cell assembly. The reference, counter, and working counters were played by saturated calomel electrode (SCE), graphite rod, and P110 steel. The experiment was performed at 308 K temperature. Autolab Nova 2.1.2 was used for electrochemical data analysis. The SCE is composed of mercurous chloride (Hg_2Cl_2, calomel) in contact with a mercury pool. These components are layered under a saturated solution of potassium chloride (KCl) with a concentration of 4 M KCl.

The EIS experiments were performed using a 10 mV AC signal using a 100 kHz to 0.01 Hz frequency range. The PDP experiments were launched in the potential range of −250 mV to +250 mV relative to OCP, applying a scan rate of 0.1 mVs^{-1}. The linear Tafel segments of anodic and cathodic curves were extrapolated to obtain corrosion current densities (i_{corr}) and anodic and cathodic Tafel slope values. The mathematical equation used for corrosion inhibition efficiency estimation is as follows:

$$\eta_{EIS} = \frac{R_{ct(inh)} - R}{R_{ct(inh)}} \times 100 \tag{3}$$

$$\eta_{PDP} = \frac{i_{corr} - i_{corr(inh)}}{i_{corr}} \times 100 \tag{4}$$

where R = resistance of charge transfer without GG-EEA, $R_{ct(inh)}$ = resistance of charge transfer with GG-EEA, i_{corr} = corrosion current density without GG-EEA, and $i_{corr(inh)}$ = corrosion current density with GG-EEA.

Analysis of surface morphology

The surface morphological analysis was done by immersing the P110 steel samples into 15% HCl solution at 308 K for 6 h without and with optimum concentration (500 mg/L) of GG-EEA for SEM, EDX, and AFM. The SEM analysis was done using Zeiss Evo 50 XVP that is coupled with EDX. The magnification used was 5 KX and 20 kV of accelerating voltage. AFM was analyzed using NT-multimode instrument, with the P110 steel dimension of 10 × 10 μm. XPS was performed using VG ESCALAB 220 XL spectrometer.

Computational details

Density Functional Theory (DFT) was used for the calculation of some important quantum chemical descriptors like hardness (η), softness (σ), electronegativity (χ), chemical potential (μ). In theory, the reactivity above descriptors is presented via the following equations based on total electronic energy (E), the number of electrons (N), ionization energy (I), and electron affinity (A) [30].

$$\mu = -\chi = \left[\frac{\partial E}{\partial N}\right]_{\nu(r)} = -\left(\frac{I+A}{2}\right) \tag{5}$$

$$\eta = \frac{1}{2}\left[\frac{\partial^2 E}{\partial N^2}\right]_{\nu(r)} = \frac{I-A}{2} \tag{6}$$

$$\sigma = 1/\eta \tag{7}$$

According to Koopmans Theorem [31], the values of HOMO and LUMO orbital energies corresponds to ionization energy and electron affinity of molecules, respectively, and given as follows:

$$I = -E_{HOMO} \tag{8}$$

$$A = -E_{LUMO} \tag{9}$$

Parr, Szentpaly, and Liu [32] modeled the electrophilicity index (ω) that gives essential clues about molecules' electrophilic characters based on chemical hardness electronegativity via the following equation.

$$\omega = \chi^2/2\eta \tag{10}$$

Chattaraj defined the nucleophilicity (ε) as the multiplicative inverse of the electrophilicity index.

$$\varepsilon = 1/\omega \tag{11}$$

Within the framework of Gazquez's study [33], the electron-accepting (ω^+) and electron-donating (ω^-) powers depend on ionization energy and electron affinities of the inhibitor molecules and are estimated as follows.

$$\omega^+ = (I + 3A)^2 / (16(I - A)) \tag{12}$$

$$\omega^- = (3I + A)^2 / (16(I - A)) \tag{13}$$

Polarizability (α), one of the useful reactivity descriptors, is calculated depending on the polarizability tensor's diagonal components.

$$\langle \alpha \rangle = 1/3\left[\alpha_{xx} + \alpha_{yy} + \alpha_{zz}\right] \tag{14}$$

The quantum chemical calculations were performed using DFT/B3LYP/6-31G/6-31G(d)/6−31++G(d) level [34].

Molecular Dynamics Simulation

Materials Studio software (Accelrys, Inc.) was used to simulate the GG and GG-EEA molecules' adsorption interaction with the metal oxide surface. The Forcite module was applied to optimize (i.e., energy minimizing) GG derivative molecules, and the Condensed- Phase Optimized Molecular Potentials for Atomistic Simulation Studies (COMPASS) [35] was used as a force field, as shown in Fig. 1. Van der Waals and electrostatic were set as atom-based summation method and Ewald summation method, respectively. The unit cell structure of Fe with the associated experimental lattice parameters is available from Materials Studio, and it was chosen for this simulation. The cell was optimized then was cleaved accordion to desired planes hkl (110). The size of the produced surface must be increased to be able to accommodate the molecules. Thus, the

Supercell tool was used to enlarge (10×10) the surface. After that, a vacuum slab with 50 Å thickness was built above the Fe (110) plane. A vacuum slab is great enough, so the GG and GG-EEA do not interact with the Fe surface's bottom layer's periodic image. The molecules of water and hydrochloric acid were sketched and optimized using the Forcite module. The Fe surface box was packed with optimized H_2O and HCl molecules using Amorphous cell modules in a specified composition (15% HCl and 85% H_2O). The simulation of the interaction of GG derivatives and Fe surface were performed in a simulation box $(35 \times 35 \times 41$ Å). To calculate adsorption (E_{ads}) and binding energies (E_{bind}), the following equations were used.

$$E_{ads} = E_{total} - \left(E_{surf+solu} + E_{inh+solu}\right) + E_{solu} \tag{15}$$

$$E_{bind} = -E_{ads} \tag{16}$$

wherein, E_{total} denotes the total energy of the studied system, $E_{surf+solu}$ represents the total energy of Fe (110) surface and solution without the inhibitor, $E_{inh+solu}$ stands for the total energy of the inhibitor and solution, and E_{solu} is the total energy of the solution.

Results and discussion

Characterization of GG-EEA

Fig. 2a represents the IR spectra of guar gum (GG). In this, a strong, wide band at 3462 represents the $-OH$ stretching in guar gum. Additionally, a weak peak at 2926 cm^{-1} corresponds to CH chains, and a peak at 1639 cm^{-1} is vibrational peaks of six-membered rings in guar gum. However, in the IR spectrum of GG-EEA (Fig. 2b) and several peaks that appear in the guar gum, an additional carbonyl peak can be seen at 1735 cm^{-1}. Also, two peaks at 2926 cm^{-1} and 2855 cm^{-1} represents the methyl CH asymmetrical and symmetrical stretching, respectively, of EEA. This confirms the grafting of ethyl acrylate (EEA) with guar gum (GG).
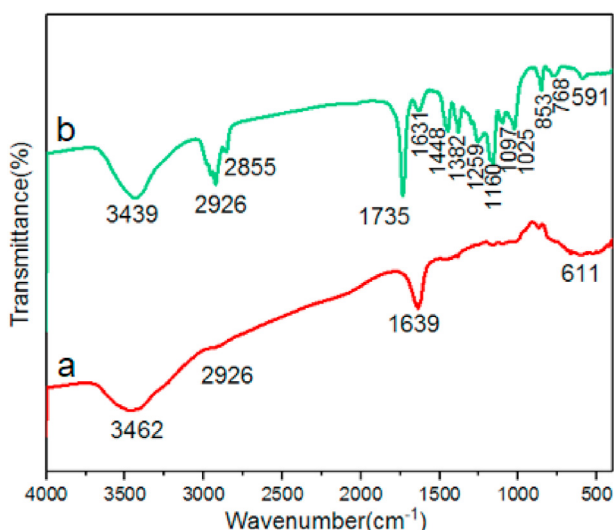

Fig. 2 − IR spectra of (a) GG (b) GG-EEA.

Weight loss experiments

Effect of concentration on inhibition efficiency (η%) and corrosion rate (C_R)

The concertation variation of GG-EEA and GG over the η% and C_R are tabulated in Table S1 (supplementary file) and shown in Fig. 3a. The figure's inspection reveals that GG-EEA acts as an excellent corrosion inhibitor in 15% HCl at 308 K temperature compared to GG. Additionally, the increasing η% and decreasing C_R values suggest the GG-EEA's effectiveness, and these values reached 92.3% and 3.2 mm/y, respectively, at only 500 mg/L. GG-EEA's corrosion protection ability is due to the formation of an adsorptive layer of GG-EEA molecules over the active sites presenting over the surface of P110 steel [36]. The optimum concentration of GG-EEA, i.e., 500 mg/L, was selected by increasing GG-EEA concentration up to 600 mg/L, and no significant change was observed.

Effect of temperature

The optimum concentration of GG-EEA was used to study the temperature effect, i.e., 308 K–348 K (Fig. S1a). The figure's observation reveals that the inhibition efficiency values decreased with an increase in temperature, which is because of GG-EEA desorption from the surface of P110 steel [37].

The application of the Arrhenius equation was used to find out the corrosion rate dependency with temperature [37]:

$$\log C_R = \frac{-E_a}{2.303RT} \tag{17}$$

where E_a = activation energy R = universal gas constant and T = temperature. Ea's value was calculated by making a plot between the log C_R vs. 1/T (Fig. S1b). The obtained value of E_a without and with GG-EEA are 67.75 kJ/mol and 34.48 kJ/mol, respectively. Notably, the addition of GG-EEA increases the E_a value, which corresponds that the energy barrier for the corrosion process has increased. However, the threshold value for chemical adsorption is 80 kJ/mol, and the calculated values are less than that. Thus, the adsorption of GG-EEA is physical adsorption at higher temperatures [38].

Adsorption study

Corrosion inhibition to protect the metal surface depends upon the adsorption strength, and that can be explained by fitting the fraction of sites (θ) occupied by the GG-EEA molecules into different isotherm models. The studied inhibitor provides the best suitable result only for the Langmuir isotherm model out of other tested different models. The criteria for selecting Langmuir are based on the closeness of R^2 and slope values near to 1 (Fig. 3b).

The equation for the Langmuir isotherm model is given below [39]:

$$\frac{C_{inh}}{\theta} = \frac{1}{K_{ads}} + C_{inh} \tag{18}$$

where C_{inh} = GG-EEA concentration (mg L^{-1}) and K_{ads} = adsorption equilibrium constant.

The K_{ads} and ΔG_{ads} are related mathematically as per the below equation [39]:

$$\Delta G_{ads} = -2.303RT \log\left(10^6 \times K_{ads}\right) \tag{19}$$
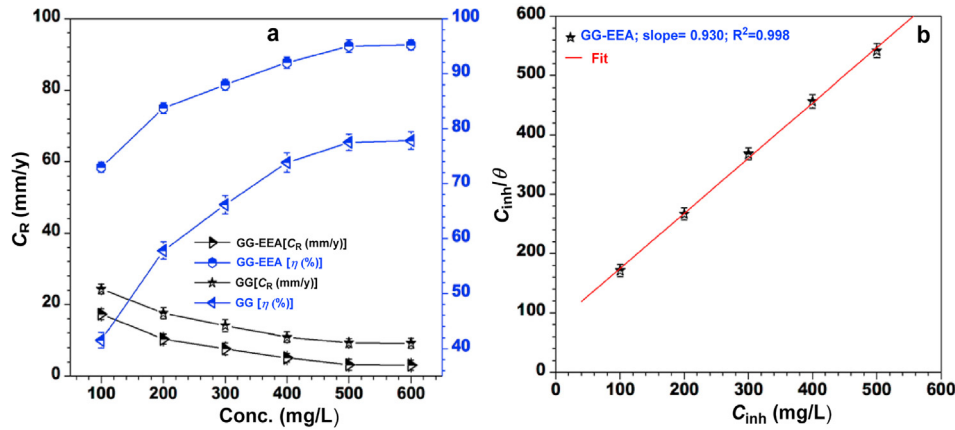
Fig. 3 — (a) Variation of inhibition efficiency (η %) and Corrosion rate (C_R) with standard deviation ($\pm$SD) **(b)** Langmuir isotherm for the adsorption of GG-EEA composite over P110 steel surface with standard deviation ($\pm$SD).

where ΔG_{ads} = adsorption free energy T = temperature R = universal gas constant and 10^6 = concentration of water. The calculated values of K_{ads} and ΔG_{ads} are 0.0122 L/mg and -24.11 kJ/mol. The calculated value of ΔG_{ads} is negative, which corresponds to the spontaneous nature of GG-EEA adsorption [39]. However, the magnitude ΔG_{ads} is coming in between -20 kJ/mol to -40 kJ/mol, which reveals combined, i.e., GG-EEA adsorption's physical and chemical nature [39].

Electrochemical studies

Electrochemical impedance analysis (EIS)

(a) Nyquist plots analysis

The fitted Nyquist plots without and with different concentrations of GG-EEA in 15% HCl solution at 308 K temperature are shown in Fig. 4a. The inspection of this figure
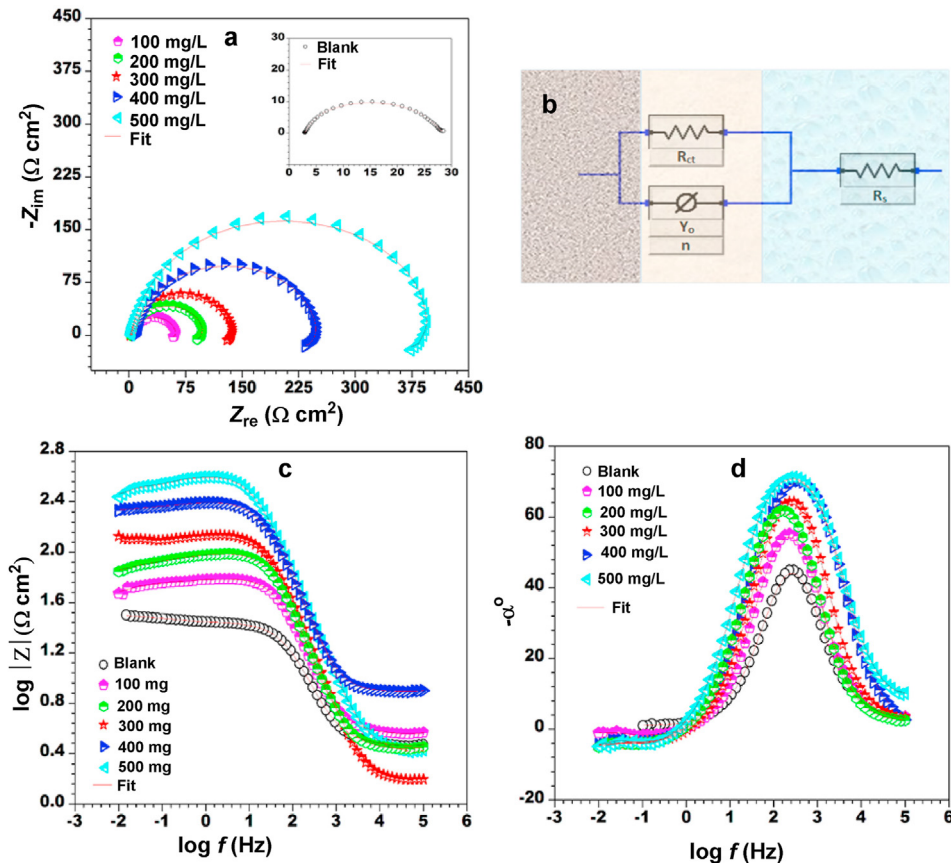

Fig. 4 — (a) Fitted Nyquist plot for P110 steel in 15% HCl without and with different concentrations of GG-EEA **(b)** Bode plots **(c)** Phase angle plots **(d)** Equivalent circuit.

represents a depressed semi-circle that is due to the surface imperfection and inhomogeneity. The semi-circle appearance also means capacitive behavior of the P110 steel both in the absence and presence of GG-EEA. It is observed that as the GG-EEA concentration increased, the size of the semi-circle increased, which is due to the increase in charge transfer resistance (R_{ct}) of the metal. Nevertheless, at optimum concertation (500 mg/L) of GG-EEA, the R_{ct} is maximum with the value of 381.7 Ω cm^2. The increment in the values of R_{ct} with the addition of GG-EEA suggests their adsorption onto the metal surface [40,41].

The equivalent circuit for exporting the data is shown in Fig. 4b. The elements that are used to construct the model of equivalent circuit are constant phase element (CPE) [42−46], charge transfer resistance (R_{ct}), and solution resistance (R_s). The double-layer capacitance (C_{dl}) and thickness of the adsorbed layer were calculated using the below equations [46]:

$$C_{dl} = (Y_o R_{ct}{}^{1-n})^{1/n} \qquad (20)$$

$$d = \frac{\varepsilon^o \varepsilon S}{C_{dl}} \qquad (21)$$

where d = thickness of the protective double-layer, ε^o = permittivity of free space, ε = dielectric constant of a solution, and S = effective surface area of the electrode. Some important calculated parameters are given in Table 1. According to the table, the values of R_{ct} and C_{dl} are increased and decreased with increasing concentration of GG-EEA. Additionally, the thickness of the double layer increased as the GG-EEA concentration increased. These observations suggest that GG-EEA adsorbed over the P110 steel surface [47,48].

In addition to this, the values of inhibition efficiency increased as the concentration of GG-EEA increased and approached a value of obtained an amount of 92.6%, which makes solid evidence of GG-EEA adsorption onto the metal surface.

(b) Bode and phase angles plots analysis

The plots of Bode and Phase angle are represented in Fig. 4c and d respectively. In Bode plots, the values of impedance modulus |Z| in the lower region of frequency are used to analyze inhibitor effectiveness performance, i.e., the more considerable the amount of |Z| more will be the corrosion resistance and higher will be the inhibition efficiency [49]. In the present, case the values of |Z| increases as the concentration of GG-EEA increases, and this confirmed the GG-EEA adsorption over the P110 steel surface [50].
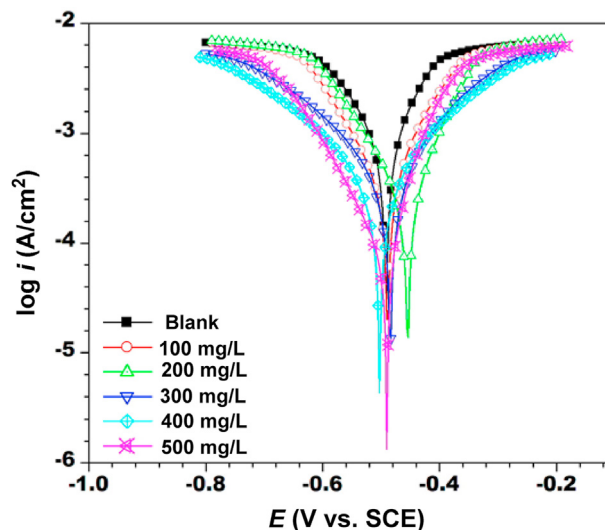

Fig. 5 − Potentiodynamic Polarization curves for P110 steel in 15% HCl without and with different concentrations of GG-EEA.

The phase angle plots suggest the increasing values of phase angles with increasing GG-EEA concentrations at an intermediate frequency, which indicates that GG-EEA molecules adsorbed over the P110 steel surface and inhibit the dissolution of metal. This information further reinforced the information gathered from Nyquist and Bode plots.

Potentiodynamic polarization measurements (PDP)
The PDP curves are shown in Fig. 5 for the corrosion of P110 steel without and with the addition of different concentrations of GG-EEA in 15% HCl solution. As can be seen from the figure that both the anodic and cathodic corrosion current values have been decreased with the addition of GG-EEA, which represents that both the anodic corrosion reactions and cathodic hydrogen evaluation reactions have been reduced with the addition of GG-EEA [51]. The parameters obtained from the PDP analysis are represented in Table 2. The values of inhibition efficiency increased, and corrosion current density decreased with the increment of GG-EEA concentration. This perhaps due to the adsorption of GG-EEA at the P110/solution interface. The highest and lowest values of i_{corr} are 221 μA/cm2 and 44 μA/cm2, respectively. Additionally, a small shift in E_{corr} values was observed in both the anodic and cathode direction, indicating the mixed nature of GG-EEA inhibition action [52].

Table 1 − **Electrochemical impedance parameters of P110 steel in 15% HCl at different concentration of GG-EEA at 308 K with standard deviation (±SD).**

C_{inh} (mg/L)	R_s (Ω cm^2)	R_{ct} (Ω cm^2)	Y_0 (Ω^{-1}s^n/cm^2)	n	Cdl μF/cm^2	η (%)
Blank	2.90	28.19 (±0.29)	380.12 (±0.81)	0.732	11360.33	–
100	3.43	60.71 (±0.41)	190.43 (±0.81)	0.799	2003.73	53.56
200	2.74	93.24 (±0.62)	152.33 (±1.09)	0.835	1007.66	69.76
300	1.38	133.24 (±0.78)	98.11 (±0.69)	0.876	375.31	78.84
400	7.80	238.85 (±0.57)	54.26 (±0.43)	0.889	177.00	88.19
500	3.12	381.76 (±0.57)	32.04 (±1.05)	0.902	89.08	92.61

It is notable from Table 2 that anodic Tafel constant values remain unchanged in the absence and presence of a different concentration of GG-EEA. This alibi GG-EEA molecules initially adsorbed over the P110 steel surface and blocked the reactive sites without altering the mechanism of anodic corrosion reactions [53]. Additionally, the cathodic Tafel constant at a lower GG-EEA concentration remains almost the same as that without GG-EEA. This suggests that at lower GG-EEA concentration, the cathodic corrosion mechanism remains the same. However, at higher GG-EEA concentration, the cathodic Tafel constant values have significantly changed compared to those without GG-EEA. This indicated that the hydrogen evolution mechanism has changed at higher GG-EEA concentration due to the barrier/diffusion effects [54]. As per Bockris and Srinivasan [55], this phenomenon is due to the decrement in the transfer coefficient of cathodic reactions. In the present case, this is due to the increase in the thickness of the double layer after more adsorption GG-EEA molecules at higher concentrations.

Surface studies

SEM and EDX analysis

The surface morphology of P110 steel using SEM before and after the immersion in 15% HCl are shown in Fig. 6a, c. The observation of P110 steel without GG-EEA addition consists of a strongly damaged surface because of the corrosive attack of aggressive media (Fig. 6a). However, after the addition of GG-EEA, the surface of metal becomes smooth due to the adsorption of GG-EEA molecules that acts as a barrier for the direct attack of aggressive media (Fig. 6c).

Fig. 6b, d and Table 3 consists of chemical compositions obtained from EDX spectrum without and with the addition of GG-EEA. In Fig. 6b, which is the EDX spectrum of the P110 steel without adding inhibitor mainly composed of O, elemental chlorine, and Fe peaks. However, after the addition of GG-EEA, the oxygen content on the surface of the sample drops sharply compared with the blank sample, no chlorine is detected, and the iron content is also obviously elevated (Fig. 6d) (Table 3). This indicates the adsorption of GG-EEA molecules on the P110 steel surface.

AFM

The surface of P110 steel without and with the addition of GG-EAA are shown as 3D and height/distance forms (Fig. 6e–h). The 3D morphological image in the absence of GG-EEA reveals a severely damaged P110 steel surface due to the direct contact between the P110 steel with the corrosive media (Fig. 6e). From the height/distance profile graph (Fig. 6f), the obtained

average roughness (R_a) is 43 nm. Nevertheless, the addition of GG-EEA causes to reduce the corrosive attack of acidic media by forming GG-EAA molecules film over the interface of P110/15% HCl, and this is supported by the smooth 3D profile of the P110 steel surface (Fig. 6g) and reduced R_a value (9.2 nm/GG-EAA) (Fig. 6h).

X-ray photoelectron spectroscopy (XPS)

The X-ray photoelectron spectroscopy (XPS) technique was used to confirm the AAP-1 adsorption and analyze the inhibitor layer's nature formed onto the surface of P110 steel in 15% HCl. The resolved XPS spectra consist of C 1s, O 1s, and Fe 2p and are shown in Fig. 7. The spectrum of Fe 2p consists of doublet peaks that are located at 711.47 ($Fe_{2p1/2}$) and 724.77 eV ($Fe_{2p3/2}$) that represents the metal surface [56]. The first peak assignment at 711.47 eV corresponds to the oxidation of iron into Fe_2O_3 and FeOOH [57]. The second peak at 724.77 eV represents Fe_2O_3 and FeO(OH), respectively [58]. The O1s deconvoluted spectra have three peaks. The peak at 530.72 eV represents O^{2-} and it means that Fe^{3+} is in the form of Fe_2O_3 and Fe_3O_4 [59]. The peak at 531.61 eV corresponds to OH^- and represents the presence of iron oxides, i.e., FeOOH [59]. The peak at 532.40 eV corresponds to oxygen molecules adsorbed in the form of water [60]. The C 1s spectra show four peaks. The peak at 284.11–284.97 eV represents C–C and C–H bonds [61]. The rise at 285.9 eV and 288.56 eV are attributed to the C–O bond and O–C=O, respectively. Thus, XPS results confirmed the GG-EEA adsorption onto the P110 steel surface.

Computational details

Frontier orbital energies are widely considered in the prediction of corrosion inhibition performances of molecules. The HOMO and LUMO structures of optimized GG and GG-EEA are shown in the supplementary file (Fig. S2). It is well-known that inhibitor molecules with high HOMO energy value act as powerful corrosion inhibitors against metal surfaces' corrosion. On the other hand, the LUMO energy level determines the electron-accepting capability of molecules. For that reason, Low E_{LUMO} values represent the inhibitor's tendency to accept electrons from the metal surface. The calculated parameters are tabulated in Table S1 (supplementary file). Within the framework of calculated frontier orbital energies, corrosion inhibition efficiency ranking of studied molecules can be given as GG-EEA > GG.

Chemical reactivity descriptors such as energy gap (ΔE), hardness, and softness are closely related parameters. Chemical hardness is defined as the resistance towards electron cloud polarization or deformation of chemical species

Table 2 – Potentiodynamic polarization parameters of P110 steel in 15% HCl at different concentration of GG-EEA at 308 K with standard deviation (±SD).

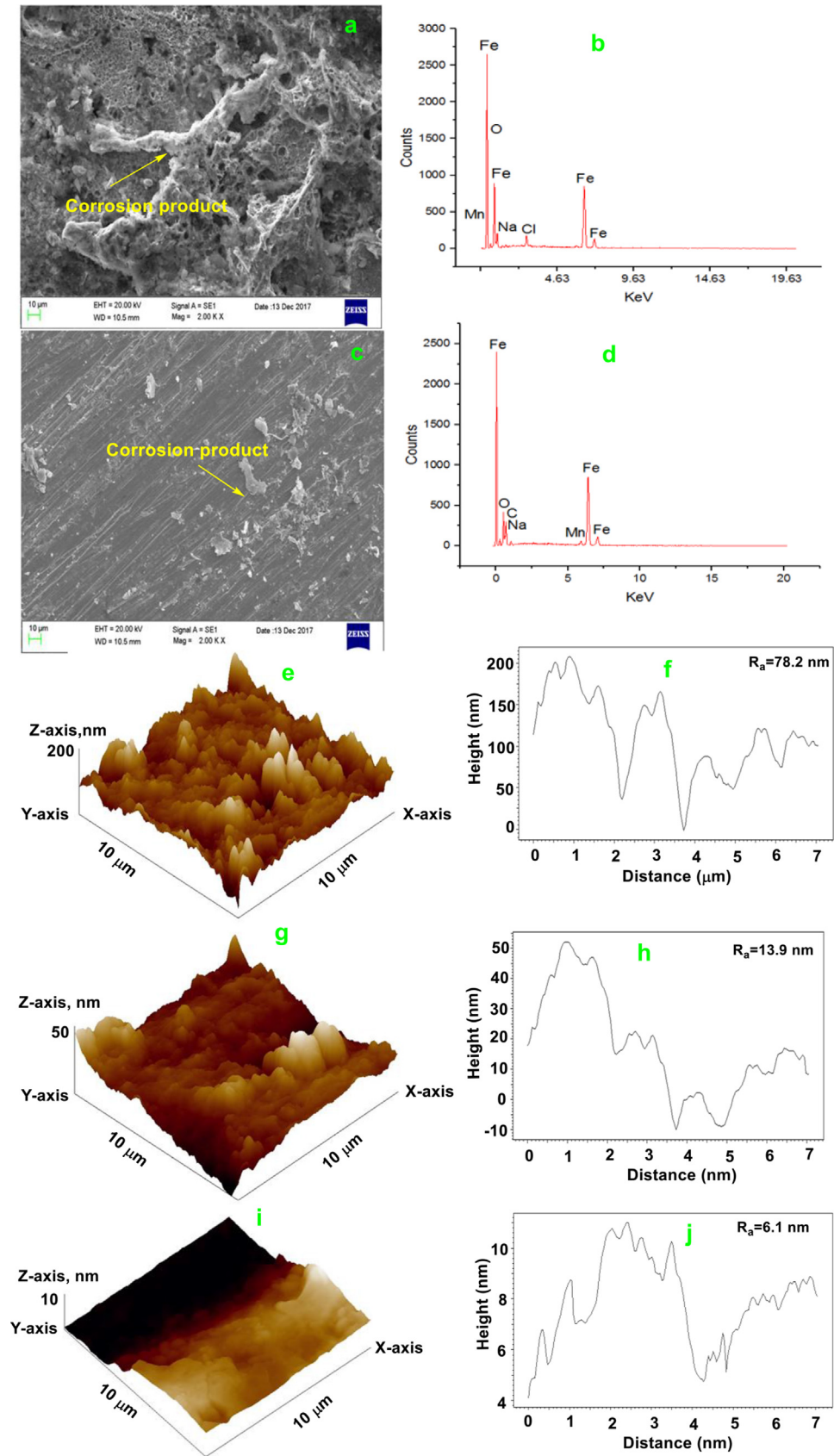| Inhibitor (mg/L)	E_{corr} (mV/SCE)	i_{corr} (μA/cm^2)	β_a (mV/dec)	$-\beta_c$ (mV/dec)	η (%)
Blank	−489	572.52 (±0.59)	112.45	85.65	–
100	−490	221.08 (±0.69)	89.30	77.32	61.38
200	−452	147.85 (±0.52)	84.53	58.55	74.17
300	−482	112.67 (±0.82)	79.93	55.72	80.32
400	−500	76.46 (±1.02)	77.15	45.41	86.64
500	−488	44.58 (±0.99)	72.05	38.09	92.21

Fig. 6 — SEM and EDX: (a, b) without GG-EEA, (c, d) with GG-EEA. Three dimension AFM images and corresponding height profile diagram: (e, f) without GG-EEA, (g, h) with GG-EEA, (i, j) abraded P110 steel.

Table 3 – Element composition of P110 steel in absence of presence of GG-EEA.

System	Fe	O	C	Cl	Na	Mn
Blank	76.62	15.04	2.86	3.35	0.54	1.59
EEA	91.55	4.39	1.81	–	1.00	1.25

Another global parameter that should be used in corrosion inhibition studies is the dipole moment. The higher value of dipole moment represents the higher adsorption of the inhibitor molecule on the metal surface. Calculated dipole moment values further support the more extraordinary adsorption ability of the GG-EEA molecule. There is a
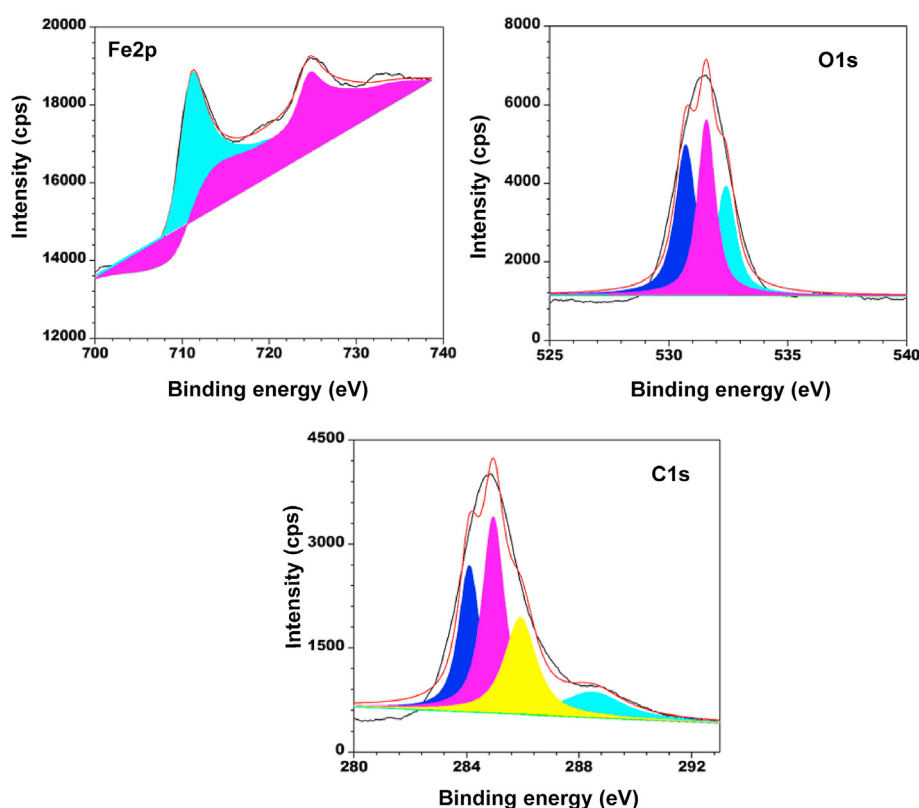
Fig. 7 – XPS spectra of inhibited P110 steel surface in presence of optimum concentration of GG-MMA.

[62]. According to the Hard and Soft Acid-Base Principle, "hard acids prefer to coordinate to hard bases, and soft acids prefer to coordinate to soft bases." Maximum Hardness Principle states that hard molecules are more stable compared to soft ones [63]. Hard molecules having high energy gap values are not useful in terms of the prevention of metal corrosion. Soft molecules are polarizable and easily give electrons to the metal surface. It is apparent from the data are given in the table that corrosion inhibition efficiency ranking obtained in the light of hardness, softness, and energy gap values of molecules can be given as GG-EEA > GG. It is important to note that this ranking is compatible with experimentally observed results.

Electron affinity, electronegativity, and electrophilicity provide useful information about molecules' electron acquisition or withdrawal powers. Molecules with high electronegativity, electrophilicity, and electron affinity values cannot exhibit effective corrosion inhibition potential. Calculated values of these parameters indicate that the GG-EEA is a better corrosion inhibitor than GG. This result is compatible with the experimentally obtained.

remarkable correlation between the dipole moment and polarizability. Minimum Polarizability Principle introduced with the help of Maximum Hardness Principle states that in stable state polarizability (α) is minimized. For that reason, according to polarizability values calculated, GG-EEA is more reactive compared to GG and acts as a better corrosion inhibitor than GG.

Molecular Dynamics Simulation (MD)

Molecular Dynamics Simulation was performed to understand the interaction between GG and GG-EEA composite molecules and metal to compare the theoretical and experimental results. The most stable adsorption configuration of GG and GG-EEA are shown in Fig. S3 a, b (Supplementary file). The adsorption energy of GG-EEA and GG are −323.52 kJ/mol, and GG is −180.37 kJ/mol, respectively. It is important to note that large negative adsorption energy values mean a more stabilized interaction between inhibitors and iron surface. It is clear that the adsorption energy of GG-EEA is more negative
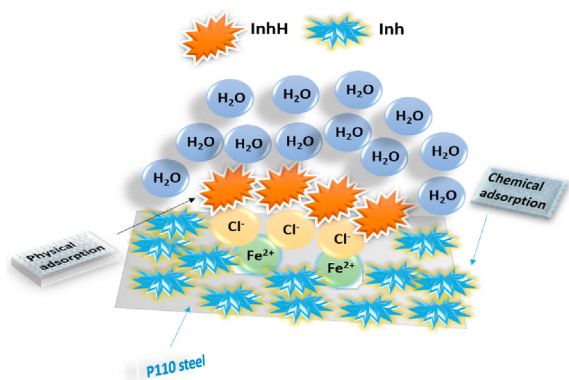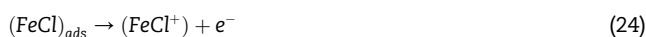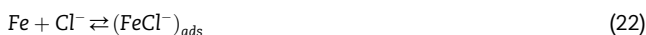
**Fig. 8 – Schematic presentation of GG-EEA adsorption over the P110 steel surface.**

than GG, and therefore GG-EEA exhibited greater inhibition abilities as compared to the GG.

Mechanism of GG-EEA adsorption

From the results of PDP, it is confirmed that GG-EEA is a mixed type of inhibitor. Additionally, the magnitude of ΔG°_{ads} further confirmed both the chemical and physical (mixed) nature of adsorption. Thus inhibitor molecules based on these results the mechanism of P110 steel dissolution at the anodic site in HCl solution is represented as follows:

$$Fe + Cl^- \rightleftharpoons (FeCl^-)_{ads} \tag{22}$$

$$(FeCl^-)_{ads} \rightleftharpoons (FeCl)_{ads} + e^- \tag{23}$$

$$(FeCl)_{ads} \rightarrow (FeCl^+) + e^- \tag{24}$$

$$(FeCl^+) \rightleftharpoons Fe^{2+} + Cl^- \tag{25}$$

Thus, the protonated inhibitor molecules (GG-EEAH$^+$) adsorbed at the anodic site as per the below reaction:

$$(FeCl^-)_{ads} + GG - EEAH^+ \rightarrow (FeCl^- GG - EEAH^+)_{ads} \tag{26}$$
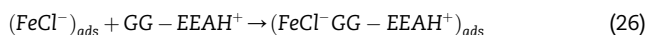
Therefore, the protonated inhibitor (GG-EEAH$^+$) from Eq. (26) can electrostatically adsorb on the P110 steel surface [64] and thus prevents the anodic corrosion reaction.

Similarly, the cathodic reaction mechanism is as follows:

$$Fe + H^+ \rightleftharpoons (FeH^+)_{ads} \tag{27}$$

$$(FeH^+)_{ads} + e^- \rightarrow (FeH)_{ads} \tag{28}$$

$$(FeH)_{ads} + H^+ + e^- \rightarrow Fe + H_2 \tag{29}$$

The protonated inhibitor molecules are also adsorbing at the cathodic sites and started doing completion with H$^+$ for electrons, thus reducing the H$_2$ evolution.

The adsorption of GG-EEA using the chemical process starts with the displacement of pre-adsorbed water molecules from the P110 steel/solution interface. The GG-EEA molecules donate the lone pair of electrons presenting over the heteroatoms to the unoccupied Fe orbitals and form coordinate/

chemical bonds [65]. The adsorption mechanism is shown in Fig. 8.

Conclusion

GG-EEA composite performance is better even at low concentrations than the earlier reported corrosion inhibitors in an acidizing environment [66–72]. The GG-EEA molecule acts by adsorbing on the P110 steel surface and obeys the Langmuir adsorption isotherm. The inhibition efficiency rose with increment in the inhibitor concentration with a maximum value of 92.3% at 500 mg/L. The thermodynamic parameters showed that GG-EEA shows a mixed-mode of physical and chemical adsorption [73–75]. EIS studies supported the inhibitor's adsorption on the steel surface, revealing a charge transfer control of the process, showing an increase in the charge transfer resistance. The PDP studies revealed that the corrosion current densities showed a decreasing trend with the inhibitor molecule's addition to the corrosive electrolyte, and the inhibitor is mixed. The Scanning electron microscope (SEM), Energy dispersive x-ray spectroscopy (EDX), Atomic force microscopy (AFM), and X-ray photoelectron spectroscopy analysis supported the adsorption of the inhibitor on the metallic surface and the formation of a protective film, which showed an improvement in the surface smoothness of the metallic surface. MD results further confirm the better adsorption of GG-EEA composite than GG alone. The developed GG-EEA composite can be a potential candidate for the petroleum industry during the acidizing process. In the future, the corrosion inhibition ability of GG-EEA can be improved for application in high-temperature wells by developing new formulations. The synthesized composite acts as a major corrosion inhibitor for P110 steel in 15% HCl.

Declaration of competing interest

The authors declare that they have no known competing financial interests or personal relationships that could have appeared to influence the work reported in this paper.

Acknowledgment

Appendix A. Supplementary data

Supplementary data to this article can be found online at https://doi.org/10.1016/j.ijhydene.2020.12.103.

REFERENCES

[1] Smith L. Control of corrosion in oil and gas production tubing. Br Corrosion J 1999;1999(34):247–53.

[2] G Bereket E Hür, Öğretir C. Quantum chemical studies on some imidazole derivatives as corrosion inhibitors for iron in acidic medium. J Mol Struct. THEOCHEM. 2002;578:79–88.

[3] El-rehim SS, Refaey SAM, Taha F. Corrosion inhibition of mild steel in acidic medium using 2-amino thiophenoland 2-cyanomethyl benzothiazole. J Appl Electrochem 2001;31:429–35.

[4] Tasic ZZ, Mihajlovic MBP, Antonijevic MM. The influence of chloride ions on the anti-corrosion ability of binary inhibitor system of 5-methyl-1H-benzotriazole and potassium sorbate in sulfuric acid solution. J Mol Liq 2016;222:1–7.

[5] Herrag L, Chetouani A, Elkadiri S. Pyrazole derivatives as corrosion inhibitors for steel in hydrochloric acid. Port Electrochim Acta 2008;26:211–20.

[6] Elewady GY. Pyrimidine derivatives as corrosion inhibitors for carbon-steel in 2M hydrochloric acid solution. Int J Electrochem Sci 2008;3:1149–61.

[7] El Azzouzi M, Aouniti A, Tighadouin S, et al. Some hydrazine derivatives as corrosion inhibitors for mild steel in 1.0 M HCl: weight loss, electrochemichal, SEM and theoretical studies. J Mol Liq 2016;221:633–41.

[8] Saha SK, Dutta A, Ghosh P. Novel Schiff-base molecules as efficient corrosion inhibitors for mild steel surface in 1 M HCl medium: experimental and theoretical approach. Phys Chem Chem Phys 2016;18:17898–911.

[9] Ashassi-Sorkhabi H, Majidi MR, Seyyedi K. Investigation of inhibition effect of some amino acids against steel corrosion in HCl solution. Appl Surf Sci 2004;225:176–85.

[10] Umoren SA. Inhibition of aluminium and mild steel corrosion in acidic medium using Gum Arabic. Cellulose 2008;15:751–61.

[11] Abdallah M. Guar gum as corrosion inhibitor for carbon steel in sulfuric acid solutions. Port Electrochim Acta 2004;22:161–75.

[12] Rajeswari V, Kesavan D, Gopiraman M. Physicochemical studies of glucose, gellan gum, and hydroxypropyl cellulose – inhibition of cast iron corrosion. Carbohydr Polym 2013;95:288–94.

[13] Li X, Deng S. Cassava starch graft copolymer as an eco-friendly corrosion inhibitor for steel in H2SO4 solution. Kor J Chem Eng 2015;32:2347–54.

[14] Fiori-Bimbi MV, Alvarez PE, Vaca H. Corrosion inhibition of mild steel in HCL solution by pectin. Corrosion Sci 2015;92:192–9.

[15] Fares MM, Maayta AK, Al-Mustafa JA. Corrosion inhibition of iota-carrageenan natural polymer on aluminum in presence of zwitterion mediator in HCl media. Corrosion Sci 2012;65:223–30.

[16] Bobina M, Kellenberger A, Millet J. Corrosion resistance of carbon steel in weak acid solutions in the presence of l-histidine as corrosion inhibitor. Corrosion Sci 2013;69:389–95.

[17] Abiola OK, James AO. The effects of Aloe vera extract on corrosion and kinetics of corrosion process of zinc in HCl solution. Corrosion Sci 2010;52:661–4.

[18] Emranuzzaman T Kumar, Vishwanatham S. Synergistic effects of formaldehyde and alcoholic extract of plant leaves for protection of N80 steel in 15%HCl. Corrosion Eng Sci Technol 2004;39:327–32.

[19] Matad PB, Mokshanatha PB, Hebbar N. Ketosulfone drug as a green corrosion inhibitor for mild steel in acidic medium. Ind Eng Chem Res 2014;53:8436–44.

[20] Eddy NO, Odiongenyi AO, Ameh PO, Ebenso EE. Corrosion inhibition potential of Daniella Oliverri gum exudate for mild steel in acidic medium. International Journal of Electrochemical Science 2012;7:7425–39.

[21] Jyothi S, Ravichandran J. Luffa aegyptiaca leaves extract as corrosion inhibitor for mild steel in hydrochloric acid medium. J Adhes Sci Technol 2014;28:2347–63.

[22] Krishnaveni K, Ravichandran J. Aqueous extract of leaves of Morinda tinctoria as a corrosion inhibitor for aluminum in sulphuric acid medium. J Adhes Sci Technol 2015;29:1465–82.

[23] Banerjee S, Srivastava V, Singh MM. Chemically modified natural polysaccharide as green corrosion inhibitor for mild steel in acidic medium. Corrosion Sci 2012;59:35–41.

[24] Roy P, Karfa P, Adhikari U. Corrosion inhibition of mild steel in acidic medium by polyacrylamide grafted guar gum with various grafting percentage: effect of intramolecular synergism. Corrosion Sci 2014;88:246–53.

[25] Biswas A, Pal S, Udayabhanu G. Experimental and theoretical studies of xanthan gum and its graft co-polymer as corrosion inhibitor for mild steel in 15% HCl. Appl Surf Sci 2015;353:173–83.

[26] Biswas Amrita, Pal Sagar, Udayabhanu G. Effect of chemical modification of a natural polysaccharide on its inhibitory action on mild steel in 15% HCl solution. J Adhes Sci Technol 2017;31:2468–89.

[27] Mudgil D, Barak S, Khatkar BS, ray diffraction X-. IR spectroscopy and thermal characterization of partially hydrolyzed guar gum. Int J Biol Macromol 2012;50:1035–9.

[28] A.C.G.-o.C.o. Metals, Standard practice for preparing, cleaning, and evaluating corrosion test specimens, ASTM international2017.

[29] Dhanapala A, Rajendra Boopathy S, Balasubramanian V. Influence of pH value, chloride ion concentration and immersion time on corrosion rate of friction stir welded AZ61A magnesium alloy weldments. J Alloys Compd 2012;523:49–60.

[30] Islam N, Kaya S. Conceptual density functional theory and its application in the chemical domain. CRC Press; 2018.

[31] Smith DW, Day OW. Extension of Koopmans' theorem. I. Derivation. J Chem Phys 1975;62:113–4.

[32] Parr RG, Szentpaly LV, Liu S. Electrophilicity index. J Am Chem Soc 1999;121:1922–4.

[33] Gazquez JL, Cedillo A, Vela A. Electro donating and electro accepting powers. J Phys Chem 2007;111:1966–70.

[34] Klein E, Lukeš V, Ilčin M. DFT/B3LYP study of tocopherols and chromans antioxidant action energetics. Chem Phys 2007;336:51–7.

[35] Guo L, Obot IB, Zheng X, Shen X, Qiang Y, Kaya S, Kaya C. Theoretical insight into an empirical rule about organic corrosion inhibitors containing nitrogen, oxygen, and sulfur atoms. Appl Surf Sci 2017;406:301–6.

[36] Solmaz R. Investigation of adsorption and corrosion inhibition of mild steel in hydrochloric acid solution by 5-(4-Dimethylaminobenzylidene) rhodanine. Corrosion Sci 2014;79:169–76.

[37] Fragoza-Mar L, Olivares-Xometl O, Domínguez-Aguilar MA, Flores EA, Arellanes-Lozada P, Jiménez-Cruz F. Corrosion inhibitor activity of 1,3-diketone malonates for mild steel in aqueous hydrochloric acid solution. Corrosion Sci 2012;61:171–84.

[38] Hamdy A, El-Gendy N Sh. Thermodynamic, adsorption and electrochemical studies for corrosion inhibition of carbon steel by henna extract in acid medium. Egyptian Journal of Petroleum 2013;22:17–25.

[39] Singh A, Ansari KR, Chauhan DS, Quraishi MA, Lgaz H. Ill-Min Chung, Comprehensive investigation of steel corrosion inhibition at macro/micro level by ecofriendly green

corrosion inhibitor in 15% HCl medium. J Colloid Interface Sci 2020;560:225–36.

[40] ElBelghiti M, Karzazi Y, Dafali A, Hammouti B, Bentiss F, Obot I, Bahadur I, Ebenso E. Experimental, quantum chemical and Monte Carlo simulation studies of 3, 5-disubstituted-4-amino-1, 2, 4-triazoles as corrosion inhibitors on mild steel in acidic medium. J Mol Liq 2016;218:281–93.

[41] Elmi F, Gharakhani A, Ghasemi S, Alinezhad H. Self-assemble l-glycine and l-cysteine/polydopamine nanohybrid films coated on 304 stainless steel for corrosion study in sterile seawater. Prog Org Coating 2018;119:127–37.

[42] Kowsari E, Arman SY, Shahini MH, Zandi H, Ehsani A, Naderi R, PourghasemiHanza A, Mehdipour M. In situ synthesis, electrochemical and quantum chemical analysis of an amino acid-derived ionic liquid inhibitor for corrosion protection of mild steel in 1M HCl solution. Corrosion Sci 2016;112:73–85.

[43] Ehsani A, Mahjani MG, Moshrefi R, Mostaanzadeh H, Shayeh JS. Electrochemical and DFT study on the inhibition of 316L stainless steel corrosion in acidic medium by 1-(4-nitrophenyl)-5-amino-1H-tetrazole. RSC Adv 2014;4:20031–7.

[44] Ehsani A, Mahjani MG, Nasseri M, Jafarian M. Influence of electrosynthesis conditions and Al2O3 nanoparticles on corrosion protection effect of polypyrrole films. Anti-corrosion Methods & Mater 2014;61:146–52.

[45] Beikmohammadi M, Fotouhi L, Ehsani A, Naseri M. Potentiodynamic and electrochemical impedance spectroscopy study of anticorrosive properties of p-type conductive polymer/TiO2 nanoparticles. Solid State Ionics 2018;324:138–43.

[46] Hosseini M, Fotouhi L, Ehsani A, Naseri M. Enhancement of corrosion resistance of polypyrrole using metal oxide nanoparticles: potentiodynamic and electrochemical impedance spectroscopy study. J Colloid Interface Sci 2017;505:213–9.

[47] Jiang L, Qiang Y, Lei Z, Wang J, Qin Z, Xiang B. Excellent corrosion inhibition performance of novel quinoline derivatives on mild steel in HCl media: experimental and computational investigations. J Mol Liq 2018;255:53–63.

[48] Qiang Y, Zhang S, Xu S, Li W. Experimental and theoretical studies on the corrosion inhibition of copper by two indazole derivatives in 3.0% NaCl solution. J Colloid Interface Sci 2016;472:52–9.

[49] Hegazy MA, Hasan AM, Emara MM, et al. Evaluating four synthesized Schiff bases as corrosion inhibitors on the carbon steel in 1 M hydrochloric acid. Corrosion Sci 2012;65:67–76.

[50] Tawfik SM. Alginate surfactant derivatives as an ecofriendly corrosion inhibitor for carbon steel in acidic environments. RSC Adv 2015;5:104535–50.

[51] Bockris JOM, Yang B. The mechanism of corrosion inhibition of iron in acid solution by acetylenic alcohols. J Electrochem Soc 1991;138:2237–52.

[52] Lyberatos G, Kobotiatis L. Inhibition of aluminum 7075 alloy corrosion by the concerted action of nitrate and oxalate salts. Corrosion 1991;47:820–4.

[53] Abdel-Rehim SS, Ibrahim MAM, Khaled KF. The inhibition of 4-(2′-amino-5′-methylphenylazo) antipyrine on corrosion of mild steel in HCl solution. Mater Chem Phys 2001;70:268–73.

[54] Zucchi F, Zucchini G, Trabanelli G. Proceedings of 3rd European symposium corrosion. Inhibitors. Ferrara, Italy: University of Ferrara; 1970. p. 121.

[55] Bockris JO'M, Srinivasan S. Elucidation of the mechanism of electrolytic hydrogen evolution by the use of H-T separation factors. Electrochim Acta 1964;9:31–44.

[56] Zhang Z, Chen S, Li Y, Li S, Wang L. A study of the inhibition of iron corrosion by imidazole and its derivatives self-assembled films. Corrosion Sci 2009;51:291–300.

[57] Nakayama N, Obuchi A. Inhibitory effects of 5-aminouracil on cathodic reactions of steels in saturated Ca(OH)2 solutions. Corrosion Sci 2003;45:2075–92.

[58] Grosvenor AP, Kobe BA, Biesinger MC, McIntyre NS. Investigation of multiplet splitting of Fe 2p XPS spectra and bonding in iron compounds. Surf Interface Anal 2004;36:1564–74. https://doi.org/10.1002/sia.1984.

[59] Temesghen W, Sherwood P. Analytical utility of valence band X-ray photoelectron spectroscopy of iron and its oxides, with spectral interpretation by cluster and band structure calculations. Anal Bioanal Chem 2002;373:601–8.

[60] Babić-Samardžija K, Lupu C, Hackerman N, Barron AR, Luttge A. Inhibitive properties and surface morphology of a group of heterocyclic diazoles as inhibitors for acidic iron corrosion. Langmuir 2005;21:12187–96.

[61] Bentiss F, Jama C, Mernari B, El Attari H, El Kadi L, Lebrini M, Traisnel M, Lagrenée M. Corrosion control of mild steel using 3, 5-bis (4-methoxyphenyl)-4-amino-1, 2, 4-triazole in normal hydrochloric acid medium. Corrosion Sci 2009;51:1628–35.

[62] Kaya S, Kaya C. A new equation for calculation of chemical hardness of groups and molecules. Mol Phys 2015;113:1311–9.

[63] Kaya S, Kaya C. A simple method for the calculation of lattice energies of inorganic ionic crystals based on the chemical hardness. Inorg Chem 2015;54:8207–13.

[64] Alhaffara MT, Umoren SA, Obot IB, Ali SA, Solomon MM. Studies of the anticorrosion property of a newly synthesized Green isoxazolidine for API 5L X60 steel in acid environment. J Mater Res Technol 2019;8:4399–416.

[65] Eduok U, Ohaeri E, Szpunar J. Electrochemical and surface analyses of X70 steel corrosion insimulated acid pickling medium: effect of poly (N-vinyl imidazole)grafted carboxymethyl chitosan additive. Electrochim Acta 2018;278:302–12.

[66] Quadri TW, Olasunkanmi LO, Fayemi OE, Solomon MM, Ebenso EE. Zinc oxide nanocomposites of selected polymers: synthesis, characterization, and corrosion inhibition studies on mild steel in HCl solution. ACS Omega 2017;2:8421–37.

[67] Solomon MM, Gerengi H, Kaya T, Umoren SA. Performance evaluation of a chitosan/silver nanoparticles composite on St37 steel corrosion in a 15% HCl solution. ACS Sustainable Chem Eng 2016;5:809–20.

[68] Solomon MM, Gerengi H, Umoren SA. Carboxymethyl cellulose/silver nanoparticles composite: synthesis, characterization and application as a benign corrosion inhibitor for St37 steel in 15% H2SO4 medium. ACS Appl Mater Interfaces 2017;9:6376–89.

[69] Solomon MM, Umoren SA, Obot IB, Sorour AA, Gerengi H. Exploration of dextran for application as corrosion inhibitor for steel in strong acid environment: effect of molecular weight, modification, and temperature on efficiency. ACS Appl Mater Interfaces 2018;10:28112–29.

[70] Wang Y, Yang Z, Zhan F, Yu ZL, Han C, Wang X, Chen W, Ding M, Wang R, Jiang Y. Indolizine quaternary ammonium salt inhibitors part II: a reinvestigation of an old-fashioned strong acid corrosion inhibitor phenacyl quinolinium bromide and its indolizine derivative. New J Chem 2018;42:12977–89.

[71] Chauhan DS, Mazumder MAJ, Quraishi MA, Ansari KR, Suleiman RK. Microwave-assisted synthesis of a new Piperonal-Chitosan Schiff base as a bio-inspired corrosion

inhibitor for oil-well acidizing. Int J Biol Macromol 2020;158:231–43.

[72] Chauhan DS, Mazumder MAJ, Quraishi MA, Ansari KR. Chitosan-cinnamaldehyde Schiff base: a bioinspired macromolecule as corrosion inhibitor for oil and gas industry. Int J Biol Macromol 2020;158:127–38.

[73] Chauhan DS, Ansari K, Sorour A, Quraishi M, Lgaz H, Salghi R. Thiosemicarbazide and thiocarbohydrazide functionalized chitosan as ecofriendly corrosion inhibitors for carbon steel in hydrochloric acid solution. Int J Biol Macromol 2018;107(B):1747–57.

[74] Singh A, Ansari K, Lin Y, Quraishi M, Lgaz H, Chung I-M. Corrosion inhibition performance of imidazolidine derivatives for J55 pipeline steel in acidic oilfield formation water: electrochemical, surface and theoretical studies. Journal of the Taiwan Institute of Chemical Engineers; 2018.

[75] Ansari K, Quraishi M, Singh A. Pyridine derivatives as corrosion inhibitors for N80 steel in 15% HCl: electrochemical, surface and quantum chemical studies. Measurement 2015;76:136–47.

NEW   The power of the Web of Science™ on your mobile device, wherever inspiration strikes.   Dismiss   Learn More

Already have a manuscript? 📁

Use our Manuscript Matcher to find the best relevant journals!

Find a Match

Filters   ☒ Clear All

Web of Science Coverage ⌄

Open Access 🔓 ⌄

Category ⌄

Country / Region ⌄

Language ⌄

Frequency ⌄

Journal Citation Reports ⌄

Refine Your Search Results

INTERNATIONAL JOURNAL OF HYDROGEN ENERGY   Search

Sort By: Relevancy ▾   ≡

Search Results

Found 3,143 results (Page 1)   ≪ **Share These Results**

Exact Match Found

INTERNATIONAL JOURNAL OF HYDROGEN ENERGY

Publisher: **PERGAMON-ELSEVIER SCIENCE LTD , THE BOULEVARD, LANGFORD LANE, KIDLINGTON, OXFORD, ENGLAND, OX5 1GB**

ISSN / eISSN: **0360-3199 / 1879-3487**

Web of Science Core Collection: **Science Citation Index Expanded**

Additional *Web of Science* Indexes: **Current Contents Engineering, Computing & Technology | Essential Science Indicators**

≪ **Share This Journal**   **View profile page**

Other Possible Matches

INTERNATIONAL ENERGY JOURNAL

Publisher: **REGIONAL ENERGY RESOURCES INFO CENTER , ASIAN INST TECHNOLOGY, PO BOX 4, KLONG LUANG, PATHUM THANI, THAILAND, 12120**

ISSN / eISSN: **1513-718X**

Web of Science Core Collection: **Emerging Sources Citation Index**

≪ **Share This Journal**   **View profile page**

INTERNATIONAL JOURNAL OF ENERGY AND ENVIRONMENTAL ENGINEERING

Publisher: **SPRINGER HEIDELBERG , TIERGARTENSTRASSE 17, HEIDELBERG,**

5

❓

Web of Science

Search   Tools ▾   Searches and alerts ▾   Search History   Marked List

Results: 1
(from Web of Science Core Collection)

You searched for: TITLE: (Chemically modified guar gum and ethyl acrylate composite as a new corrosion inhibitor for reduction in hydrogen evolution and tubular steel corrosion protection in acidic environment) ...More

🔔 Create an alert

Refine Results

Search within results for... 🔍

Publication Years ▲
☐ 2021 (1)

Refine

Web of Science Categories ▲
☐ CHEMISTRY PHYSICAL (1)
☐ ELECTROCHEMISTRY (1)
☐ ENERGY FUELS (1)

more options / values...

Refine

Document Types ▲
☐ ARTICLE (1)

Refine

Organizations-Enhanced ▲
☐ CUMHURIYET UNIVERSITY (1)
☐ KING FAHD UNIVERSITY OF PETROLEUM MINERALS (1)
☐ SOUTHWEST PETROLEUM UNIVERSITY (1)

more options / values...

Refine

Funding Agencies ▼

Authors ▼

Source Titles ▼

View all options

For advanced refine options, use

Analyze Results

Sort by: Date ⬇   Times Cited   Usage Count   Relevance   More ▾   ◀ 1 of 1 ▶

☐ Select Page   📤 Export...   Add to Marked List   📊 **Analyze Results**
                                                                      📊 **Create Citation Report**

☐ 1.   Chemically modified guar gum and ethyl acryl... reduction in hydrogen evolution and tubular s...
       By: Singh, Ambrish; Ansari, K. R.; Quraishi, M. A.; et...
       INTERNATIONAL JOURNAL OF HYDROGEN ENE...
       Published: FEB 24 2021

       View Abstract ▾

☐ Select Page   📤 Export...   Add to Marked List

Sort by: Date ⬇   Times Cited   Usage Count   Relevance

Show: 10 per page ▾

1 records matched your query of the 78,725,508 in the data limits you s...

INTERNATIONAL JOURNAL OF HYDROGEN ENERGY   ✕

Impact Factor

5.816   **5.242**
2020   5 year

JCR ® Category	Rank in Category	Quartile in Category
CHEMISTRY, PHYSICAL	48 of 162	Q2
ELECTROCHEMISTRY	9 of 29	Q2
ENERGY & FUELS	37 of 114	Q2

Data from the 2020 edition of Journal Citation Reports

Publisher
PERGAMON-ELSEVIER SCIENCE LTD, THE BOULEVARD, LANGFORD LANE, KIDLINGTON, OXFORD OX5 1GB, ENGLAND

ISSN: 0360-3199
eISSN: 1879-3487

Research Domain
Chemistry
Electrochemistry
Energy & Fuels

Close Window